AGU Advances

Supporting Information for

Unraveling the Atmospheric Energy Input and Ionization due to EMIC-Driven Electron Precipitation from ELFIN's Observations

L. Capannolo[1], R. Marshall[2], W. Li[1], G. Berland[2], K. Duderstadt[3], N. Sivadas[4,5], D. Turner[6], and V. Angelopoulos[7]

[1] Center for Space Physics, Boston University, Boston, MA, USA

[2] Department of Aerospace Engineering Sciences, University of Colorado Boulder, Boulder, CO, USA

[3] Earth Systems Research Center, The University of New Hampshire, Durham, NH, USA

[4] Space Weather Laboratory, NASA Goddard Space Flight Center, Greenbelt, MD, USA

[5] Department of Physics, The Catholic University of America, Washington DC, MD, USA

[6] Johns Hopkins University Applied Physics Laboratory: Laurel, MD, USA

[7] Department of Atmospheric and Oceanic Sciences, University of California, Los Angeles, CA.

Contents of this file

Figures S1 to S3

Introduction

This document shows 3 supporting figures. Figure S1 shows the spatial distribution of the EMIC-driven events with associated peak ionization rates and peak altitudes. Figures S2 and S3 show the ionization rate results if the input PAD is assumed realistic, isotropic or sinusoidal.

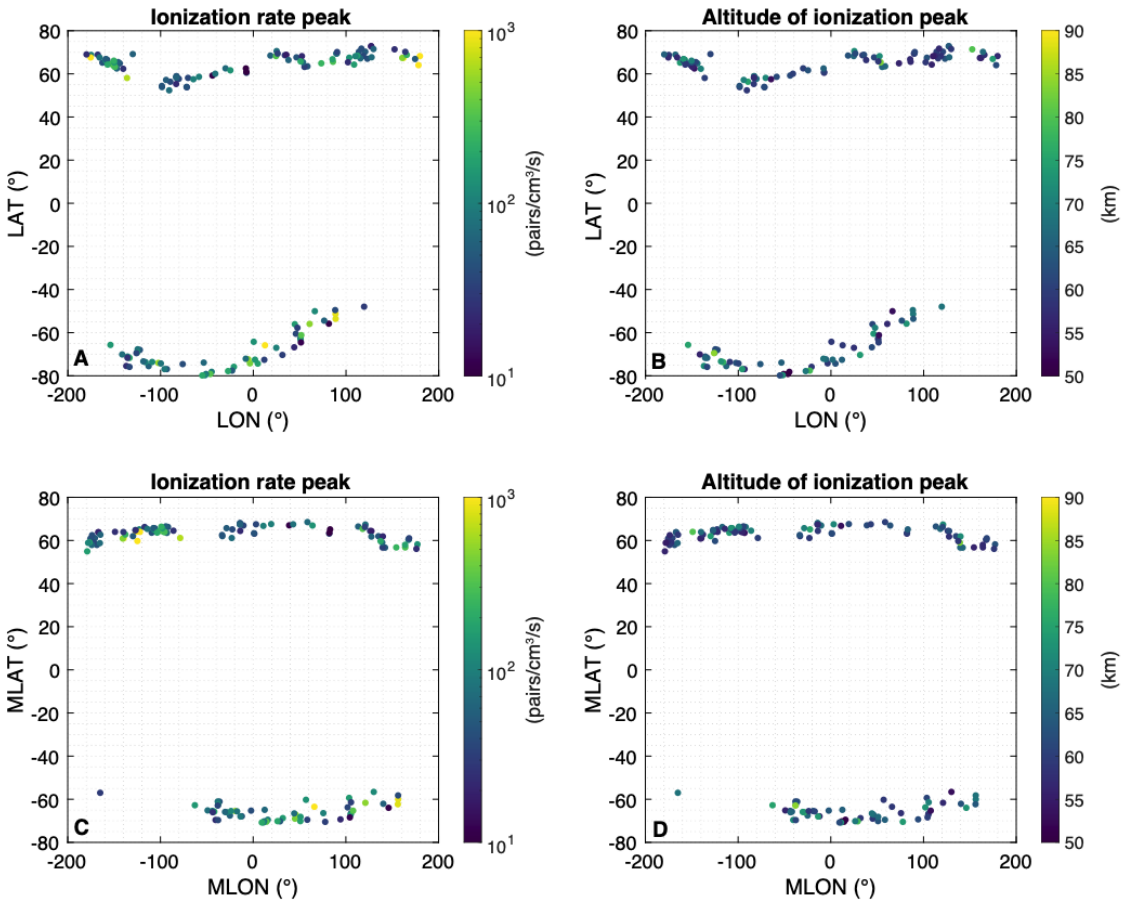
Ionization rate peak
Altitude of ionization peak
LAT (°)
LON (°)
MLAT (°)
MLON (°)
(pairs/cm³/s)
(km)
A
B
C
D

24

Figure S1. Spatial distribution of the 144 EMIC-driven precipitation events in geographical (A, B) and magnetic (C, D) coordinates. A&C: peak of ionization rate; B&D: altitude of ionization peak. No evident pattern emerges in terms of ionization peak or altitude concerning geographical or magnetic locations. This may be attributed to the relatively small statistics of the dataset and the limited L-MLT coverage of the ELFIN CubeSats. Note that our dataset encompasses years from 2019 to 2022, thus neglecting any temporal variation within this time period. Additionally, various factors influence not only the ionization rate profiles (e.g., solar conditions, atmospheric density, PAD, etc.) but also the efficiency of EMIC waves in scattering electrons (e.g., wave properties, radiation belt flux, etc.) and the available coverage of LEO spacecraft. Therefore, revealing possibly underlying trends based on geographical/magnetic coordinates poses a complex challenge, even with larger statistical datasets.

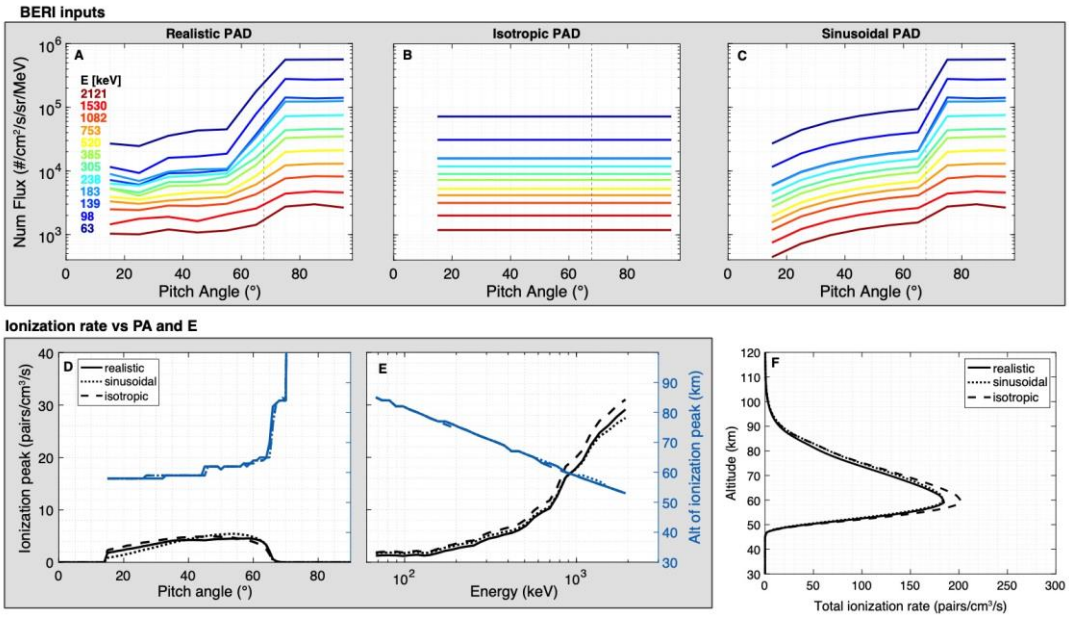

Figure S2. Comparison of ionization rates given a realistic (A), isotropic (B) or sinusoidal (C) PAD. To isolate the impact of pitch-angle variations alone and ruling out any effect due to a different input energy flux, we ensure that the energy flux inside the loss cone is equal across the chosen PAD shapes. Thus, from the realistic average PAD (A), we calculate the isotropic (B) and sinusoidal (C) PADs by conserving the energy flux in the loss cone for each energy channel. D&E: variability of the ionization peak (black) and corresponding altitude (blue) as a function of pitch-angle (D) or energy (E); F: total ionization rates in a linear scale.

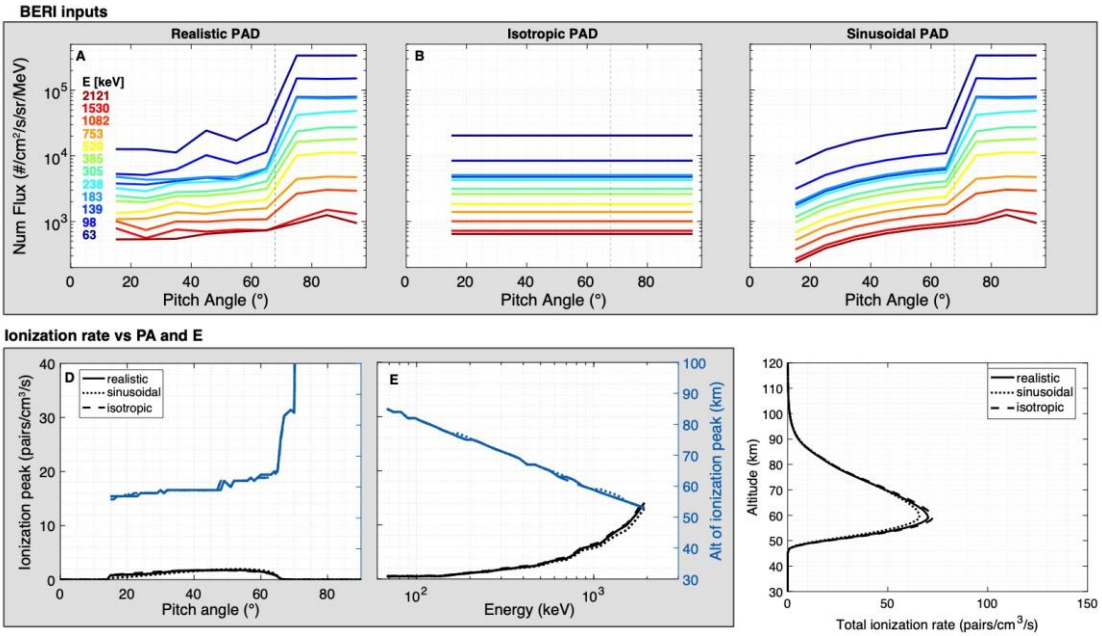

Figure S3. Same format as Supplementary Figure 2, but for the median PAD (A).